TECHNICAL UNIVERSITY OF CRETE
ELECTRONIC AND COMPUTER ENGINEERING DEPARTMENT
TELECOMMUNICATIONS DIVISION

Non-coherent Receivers for Zero-feedback Distributed Beamforming in Connectivity-constrained Wireless Sensor Networks (WSNs)

by

Alexandris Konstantinos

A THESIS SUBMITTED IN PARTIAL FULFILLMENT OF
THE REQUIREMENTS FOR THE MASTER DEGREE OF

ELECTRONIC AND COMPUTER ENGINEERING

April 2014

THESIS COMMITTEE

Associate Professor Aggelos Bletsas, *Thesis Supervisor*
Associate Professor George N. Karystinos
Professor Athanasios P. Liavas

Abstract

Power-constrained wireless sensor networks (WSNs) suffer from network partitioning problems. In many cases, each node among a network subset, cannot reliably communicate with a distant receiver even when transmitting at maximum power. Thus, a collaborative beamforming scheme among the distributed adjacent terminals is needed in terms of power addition. Prior art on distributed beamforming has mainly focused on feedback messages for channel estimation (CSI) or physical layer carrier phase adjustments. In sharp constrast, this thesis assumes commodity radios and studies the low signal to-noise-ratio (SNR) regime, where accurate channel estimation is not feasible and no reliable feedback exists. The main idea is to exploit recently proposed zero-feedback distributed beamforming and design specific non-coherent receivers. Towards that goal, three concrete non-coherent receivers are presented for zero-feedback distributed beamforming (ZF-DBF); one based on energy detection, one based on maximum-likelihood for a specific condition (i.e., full correlation among the received samples), and finally, one non-coherent receiver for all other cases. A non-coherent receiver for energy harvesting through time division multiple access (TDMA) is also provided for comparison purposes. Analytical and numerical bit-error-rate results are presented. It is shown that the ZF-DBF receiver outperforms the energy harvesting one at the low-SNR regime and overcomes connectivity adversities by exploiting signal alignment from the distributed terminals, at the expense of total (network) power transmission.

Acknowledgements

I would like to take some time here and thank the people who made the completion of this work possible. First of all, my parents, without whom my entire studies would not have been possible. I would also like to thank all my friends for encouraging and supporting me all these years. Next, I need to thank all the people who create such a good atmosphere in the lab. I also need to acknowledge my master thesis supervisor, Associate Professor Aggelos Bletsas, for all his guidance, support and patience. Finally, I would like to thank my committee members who graciously agreed to serve on my committee.

Table of Contents

List of Figures

List of Abbreviations

BER	Bit Error Rate
CFO	Carrier Frequency Offset
CSI	Channel State Information
CWGN	Complex White Gaussian Noise
MAP	Maximum-a-Posteriori probability
MIMO	Multiple-Input and Multiple-Output
ML	Maximum Likelihood
p.d.f.	probability density function
c.d.f.	cumulative distribution function
ppm	parts per million
rv	random variable
SNR	Signal to Noise Ratio
TDMA	Time Division Multiple Access
WSN	Wireless Sensor Network

Preface

Definitions, theorems, lemmas, corollaries and examples share the same index within each chapter. The symbol □ stands for the end of proof of theorem, or lemma.

x	a variable
$\mathbf{x}$	a vector
$\mathbf{A}$	a matrix
$\mathbf{A}^T$	transpose of $\mathbf{A}$
$\mathbf{A}^\dagger$	conjugate transpose of $\mathbf{A}$
$\text{rank}\,(\mathbf{A})$	the rank of matrix $\mathbf{A}$
$\mathbf{I}_N$	$N \times N$ identity matrix
$\|x\|$	the absolute value of a real or complex number
$[a/b]$	the integer division operator
$a \mod b$	the modulo operator
$a \mid b$	stands for a divides b
$a \nmid b$	stands for a does not divide b
$\|\|\mathbf{x}\|\|_2$	the $\mathcal{L}_2$ norm of a vector $\mathbf{x}$
$\mathbb{Z}$	the set of integer numbers
$\Re\,(\cdot)$	the real part of a complex number
$\Im\,(\cdot)$	the imaginary part of a complex number
$\mathcal{O}\,(\cdot)$	the order of magnitude
$\text{erfc}\,(\cdot)$	denotes the complementary error function [1]

[1] The error complementary function is given by: $\text{erfc}\,(x) = \frac{2}{\sqrt{\pi}} \int_x^{+\infty} e^{-t^2} dt$.

$\mathcal{N}(\boldsymbol{\mu}, \boldsymbol{\Sigma})$	denotes the distribution of a Gaussian random vector with mean vector $\boldsymbol{\mu}$ and covariance matrix $\boldsymbol{\Sigma}$ [2]
$\mathcal{CN}(\mathbf{0}, \boldsymbol{\Sigma})$	denotes the distribution of a circularly-symmetric complex Gaussian random vector with covariance matrix $\boldsymbol{\Sigma}$ [2]
$\mathcal{G}(k, \theta)$	denotes the Gamma distribution with parameters k, θ [2]

[2] **The closed form of the distributions is placed in Appendix A.**

Chapter 1

Introduction

1.1 Motivation

Ubiquitous wireless sensor networks (WSNs) constructed by low-cost, battery operated radio commodities equipped with isotropic antennas suffer from weak and undirected propagated signals. Distributed beamforming wireless nodes cooperatively transmit their signals in a way that their phases align and constructively offer a beamforming gain towards the desired receiver. Contrary to traditional beamforming literature and classic phased-array systems, deployed terminals are distributed at random locations and operate as independent processing units. Employing distributed antenna elements, a virtual antenna array is shaped, which offers high directivity towards the destination. In that case, several challenges, such as different carrier frequency offsets and time synchronization between the distributed terminals have to be taken into account. Power-constrained WSNs have been sparked interest on proposing new algorithms for boosting transmitting power and ensuring trustworthy connectivity, when a subset of network nodes cannot reach reliably a destination outside of this subset (i.e., reachback communication problem).

1.2 Related Work

The pre-existing literature tried to overcome a lot of beamforming schemes adversities. Several methods were proposed, including optimization based on prior knowledge, (e.g., channel state information (CSI) availability [1] or its second order statistics [2]), so as to maximize the received signal-to-noise ratio (SNR) under transmit power limitations. Another challenge, beyond

the power constraints, regards the transmitted signals phase alignment at the receiver. Phase alignment is based on carrier and packet synchronization and is fundamentally important in creating constructive beamforming gain. In a distributed environment, several challenges appear, since each node is equipped with its local oscillator and the geographical position of the nodes can be unknown. Several proposed techniques exploiting various types of feedback have been used for synchronization, i.e., full–feedback closed-loop [3], 1-bit closed-loop [4], master-slave open-loop [5], synchronization, round-trip synchronization [6] and two-way synchronization [7]. The feasibility of these techniques has been presented in several experimental prototypes [8–11]. Authors in [12, 13] introduce intermediate relay nodes with adaptively changing weights as a solution to the problems of the distributed setup. Another approach includes an interference-limited spread-spectrum scheme across the distributed nodes maintaining the beamforming properties of the network [14].

A new time and phase synchronization algorithm is presented in [15], where its precision is evaluated in multi-user multiple input-multiple output (MU-MIMO) setups using wireless open-access research platform (WARP) radios. Phase and time synchronization among the distributed transmitters is based on a master-slave architecture. A field-programmable-gate-array (FPGA) is used on each WARP for the implementation of the synchronization algorithm and signal generation. Finally, 1-bit feedback distributed beamforming [8] is revisited in [16] and a scalable architecture that is based on receiver's wireless feedback and an extended Kalman filter at the transmitters frequency locking is also discussed. An experimental validation that uses commercial software-defined radios is also included. An extended survey of distributed beamforming can be found in [17] and the references therein.

In most frequent cases, prior art requires CSI acquisition at the distributed transmitters (e.g., [18]), feedback from the receiver or carrier phase adjustments including physical layer access. Recent random matrix theoretical results [19–21] or subspace tracking methods [22] offer blind eigenvalue-based detectors which are not practicable in our case. The proposed schemes demand large amount of symbols and computational complexity in order

to ensure reliable connectivity. Information-theoretic capacity-related results for *centralized* multiple-input multiple-output (MIMO) are presented for a non-coherent reception in [23] through unitary space-time modulation (USTM) [24],[25]. Those designs support centralized multi-antenna transmitters, where no carrier frequency offset (CFO) exists among the transmitters. In our case, the distributed nature of the system assumes terminals with different local oscillators, thus different CFOs are included. For this reason, USTM is not directly applicable for the distributed transmitters setup of our case, as it was shown in [26].

1.3 Thesis problem

This section discusses the problem assumptions and presents the problem formulation described by the system model.

1.3.1 Problem assumptions

This thesis examines distributed beamforming characteristics in an unusual way. The problem becomes more challenging, including the following assumptions:

- no CSI available at the destination,
- no reliable receiver-based feedback,
- no access to the physical layer for carrier phase adjustments (low-cost off-the-shelf radio modules).

Assuming the above, huge interest is drawn for non-coherent reception, especially at low SNR regimes, where channel estimation often cannot be conducted (CSI is not available), but packet-level synchronization can be performed.

Our interest focuses on network partitioning problems, where a subset of distributed terminals cannot reach a destination outside of it. For instance, one node does not suffice to establish a reliable connection with another

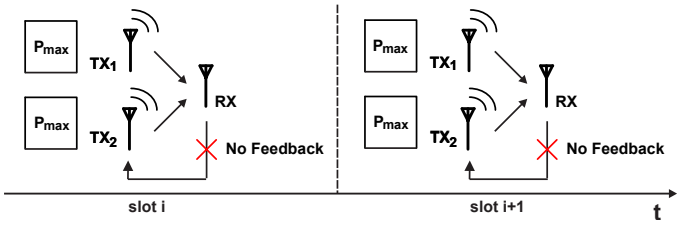

(a) Zero-feedback distributed beamforming

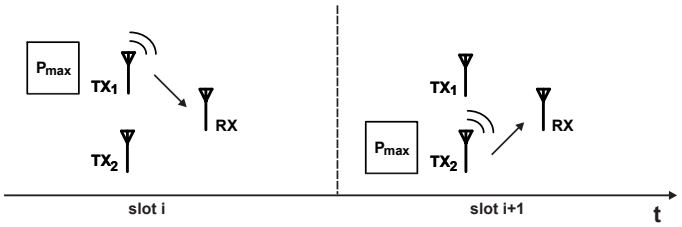

(b) TDMA

Figure 1.1: Transmission schemes

part of the network. Feedback messages cannot be received reliably and assuming low-cost commodity radios, no physical access is available. Zero-feedback beamforming with unsynchronized carriers can offer beamforming gain at receiver via a signal alignment event. Information-theoretic analysis is provided in [27],[28], showing that signal alignment is offered and signal alignment delays are computed given specific beamforming gains.

Emergency situations are assumed, where a single node transmitting at maximum power cannot reach reliably the destination. Zero-feedback beamforming technique, where each node transmitting at maximum power as referred, can be used for providing constructive gains in order to reach reliably the receiver. Another proposed technique uses the nodes transmitting in a round-robin fashion (e.g., with time division multiple access (TDMA) protocol); in this technique the receiver gathers energy from different distributed transmitters in order to achieve reliable connectivity. Hence, this thesis focuses on low SNR regimes and addresses the issue of zero-feedback distributed beamforming setup performance compared to the TDMA ones (Fig. 1.1).

1.3.2 Problem formulation and system model

M distributed terminals are synchronized in time in order to transmit the same symbol to a destination terminal at a specific frequency band (Fig. 1.2). Binary modulation scheme is assumed, specified by the signal set $\mathcal{X} = \{x_0, x_1\}$. The propagated signal between transmitter $m \in \mathcal{T} \triangleq \{1, \ldots, M\}$ and destination suffers Rayleigh, flat fading $h_m \triangleq A_m e^{j\phi_m} \sim \mathcal{CN}(0,1)$, equivalent channel taps $\{h_m\}_{m\in\mathcal{T}}$ are independent random variables for all $m \in \mathcal{T}$. Due to the fact that distributed transmitters are equipped with non-ideal local oscillators (i.e., manufacturing errors create offsets from the nominal oscillation frequency), the model introduces carrier frequency offsets (CFOs) $\{\Delta f_m\}$ independent and identically distributed (i.i.d.) random variables according to $\mathcal{N}(0, \sigma_f^2)$. The standard deviation σ_f is given by $\sigma_f = \sqrt{\mathbb{E}\left[\Delta f_m^2\right]} = f_c \times \text{ppm}$, where f_c is the nominal frequency and ppm is the frequency skew of the clock crystals, with typical values of 1-20 parts per million (ppm) ($\times 10^{-6}$). The k^{th} received signal at the destination faces additive complex Gaussian noise (CWGN) $w_k \sim \mathcal{CN}(0, \sigma^2)$ and is given by:

$$y_k \triangleq x_k \sum_{m=1}^{M} h_m e^{+j2\pi\Delta f_m k T_s} + w_k = \widetilde{x}_k + w_k, \tag{1.1}$$

where $x_k \in \mathcal{X}$ and $1/T_s$ is the symbol-transmission (baud) rate.

Parameter L denotes the number of transmitted symbols per block (block-length). "Phase" is the duration of L symbols, in which fading coefficients remain unchanged (quasi-static fading). After the end of a phase, a new one begins with completely different fading parameters. CFO parameters are considered to be constant, during one phase.[3] OOK modulation is assumed, thus the binary signal set becomes $\mathcal{X} = \{x_0, x_1\}$, where $x_0 = 0$ and $x_1 = \sqrt{E_1}$. The average signal-to-noise ratio (SNR) per m^{th} transmitter antenna per k^{th}

[3]CFO typically changes with temperature; the latter can be assumed constant for a number of transmitted bits.

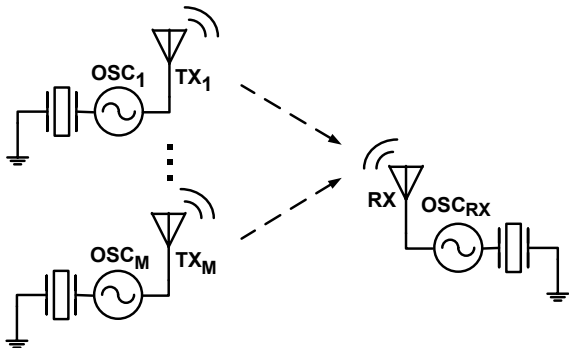

Figure 1.2: System setup with M distributed transmitters.

time slot is defined as:

$$\text{SNR} \triangleq \frac{\mathbb{E}[x_k^2]}{\mathbb{E}[|w_k|^2]} = \frac{E_1}{2\sigma^2}. \tag{1.2}$$

1.4 Thesis contributions

This work offers four concrete non-coherent detectors:

- One energy-based heuristic detector.
- One maximum-likelihood detector, derived only for a specific condition (i.e., full correlation among the received samples) and one heuristic detector in case of this condition is not satisfied. BER performance for the maximum-likelihood receiver is also enclosed.
- One energy harvesting (TDMA-based) maximum-likelihood detector and its BER performance analytical form.

Prior work in [26] presented the same energy-based heuristic detector as this work does. However, the results presented in [26] included a great amount of received samples coming from retransmissions of the same symbol in order to increase the probability of an alignment event. It was noticed

that a large number of the aggregated noise samples at receiver can be detected as constructive addition of the transmitted signals [26, Section 2.4], thus probability of false alarm increases. Additionally, a non-coherent receiver, proposed in [26], based on interleaving did not take advantage of the alignment event, but it only aimed to exploit diversity.

This work assumes high achieved rates, thus the number of retransmissions of the same symbol arrive at the receiver and the probability of false alarm remains small. All the proposed receivers beside energy harvesting (TDMA-based) receiver are based on the idea of zero-feedback beamforming exploiting the alignment event. The energy harvesting receiver proposes a different protocol where energy is collected through the distributed terminals via a time division multiplexing. Finally, this work focuses on low SNR regimes, contrary to [26], where reachback communication problem seems to be intractable. Analytical and numerical results show that zero-feedback beamforming schemes, compared to the energy harvesting one, ensure reliable connectivity and alleviate reachback connectivity adversities.

1.5 Thesis outline

Specifically, thesis outline is presented as follows:

- In Chapter 2, one heuristic receiver based on energy detection, one maximum-likelihood receiver applied only for one condition (i.e., full correlation among the received samples) and one heuristic receiver if this condition is not valid. For the maximum-likelihood receiver, bit-error-rate (BER) is analytically computed in closed form.
- In Chapter 3, a non-coherent maximum-likelihood receiver is proposed for the energy harvesting TDMA scheme and its BER performance in close form is derived.
- In Chapter 4, analytical and numerical results of the proposed receivers are presented.
- In Chapter 5, the conclusion is provided.

Chapter 2

Zero-feedback distributed beamforming receivers

This chapter discusses the idea of zero-feedback distributed beamforming (ZF-DBF) and assumes scenarios, where weak links between the receiver and all distributed terminals exist. Thus, feedback messages including CSI acquired via pilot signals or any other type of feedback messages cannot be considered. Additionally, low-cost commodity radios transmitting at maximum power are assumed without physical layer access for carrier frequency adjustments. The first part includes the basic idea of zero-feedback beamforming gain via an alignment event of the transmitted signals from distributed nodes. Numerical and analytical results on the probability of an alignment event are also contained. The second part provides one transmission protocol that exploits alignment event using repetitive transmission. Finally, three non-coherent receivers are proposed for this scheme: one heuristic based on energy detection, one maximum-likelihood only for one condition (i.e., full correlation among the received samples) and one heuristic if this condition does not hold. For the maximum-likelihood receiver, BER is analytically evaluated in closed form.

2.1 Alignment probability event

The idea behind zero-feedback distributed beamforming is based on constructive beamforming gain via a *signal alignment* at the receiver, exploiting the existence of different CFO parameters due to the distributed characteristics

of the system. The received signal power according to Eq. (1.1) is given by:

$$\begin{aligned}
|\tilde{x}_k|^2 &= \left| x_k \cdot \left(\sum_{m=1}^{M} h_m e^{+j2\pi\Delta f_m k T_s} \right) \right|^2 \\
&= x_k^2 \cdot \left| \left(\sum_{m=1}^{M} A_m e^{+j(2\pi\Delta f_m k T_s + \phi_m)} \right) \right|^2 \\
&= x_k^2 \cdot \left\{ \sum_{m=1}^{M} A_m^2 + 2 \sum_{m \neq i} A_m A_i \cos\left(2\pi \left(\Delta f_m - \Delta f_i\right) k T_s + \phi_m - \phi_i\right) \right\} \\
&= x_k^2 \cdot \mathrm{L}_{\mathrm{BF}}\left[k\right]. \qquad (2.1)
\end{aligned}$$

The sign of cosine terms inside the braces depends on the pairwise CFO and channel phase differences among the transmitting terminals. In respect to the positiveness or negativeness of the cosines, the beamforming gain $\mathrm{L}_{\mathrm{BF}}\left[k\right]$ is constructive or destructive. In other words, each m^{th} transmitted signal can be considered as a phasor $A_m e^{+j(2\pi\Delta f_m k T_s + \phi_m)}$, (see Eq. (1.1)), with angular rotating speed proportional to the respective CFO Δf_m. Then, there will be a non-zero probability that all phasors (signals) align, since the phasors rotate with different angular speeds. Here, an example is given for perfect constructive addition of the signals: two distributed transmitters ($M = 2$) have carrier frequency offsets $\Delta f_2 = 2\Delta f_1 = f_0$ and their signals arrive at the destination with phase difference π at time instant $t = t_0$. The two signals align at $t = t_0 + 1/f_0$, providing constructive addition at the destination (see Fig. 2.1). This implies that repetitive transmission of the same information symbol can offer a constructive beamforming gain via an alignment event using zero-feedback distributed beamforming scheme.

Revisiting the analysis in [27], the alignment event of M distributed transmitters is considered to occur within a sector ϕ_0. The sector $\phi_0 = \cos^{-1}(a)$ is constrained on the alignment parameter $a \in (0, 1]$.

In [27] the authors presented the alignment probability of M signals for any $M-$dimensional phase offset vector $\bar{\phi} = [\phi_1, \ldots, \phi_M]^T$ and any CFO distribution, the expected number of symbols where alignment occurs, the required average length of repetition and studied the feasibility of such schemes.

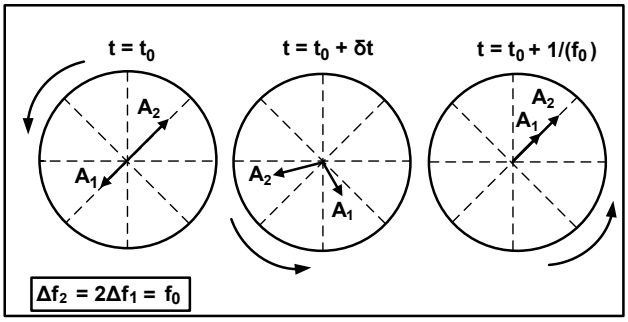

Figure 2.1: Zero-feedback distributed beamforming views transmitted signals as rotating phasors with non-zero alignment probability.

The maximum value of the beamforming factor, $\mathrm{L_{BF}}[k]$, is proved to be in the order of M^2, $\mathcal{O}(M^2)$, when the phasors are perfectly aligned ($\phi_0 = 0$).

The probability of an alignment event is numerically computed in [27]. Results in [27, Section III] provide the lower bound of the alignment probability in closed form [27, Eq. 21] via numerical and analytical computations in [27, Appendix I]. Assuming zero-mean i.i.d normal distribution for $\{\Delta f_m\}$, $m \in \mathcal{T}$, CFO parameter, 20 ppm clock frequency skew and $\phi_0 = \pi/4$, alignment probability and its lower bound are computed and depicted in Fig. 2.2. Simulations showed that lower bound is tight and analysis validates the numerical results. Finally, it is noted that alignment probability drops exponentially with the linear increment of the number M of transmitters and is constant across the time (steady-state). This implies that an alignment event is likely to occur at any time interval across the time and is more unlikely to happen as the number M of transmitters is increased.

2.2 Transmission protocol

Signal alignment event exploits repetitive transmission, as explained above. M distributed transmitters simultaneously emit the same information symbol for L slots, while the channel taps are not changed (Fig. 2.3). The achieved rate is $1/L$ and according to the system assumptions, the binary hypothesis

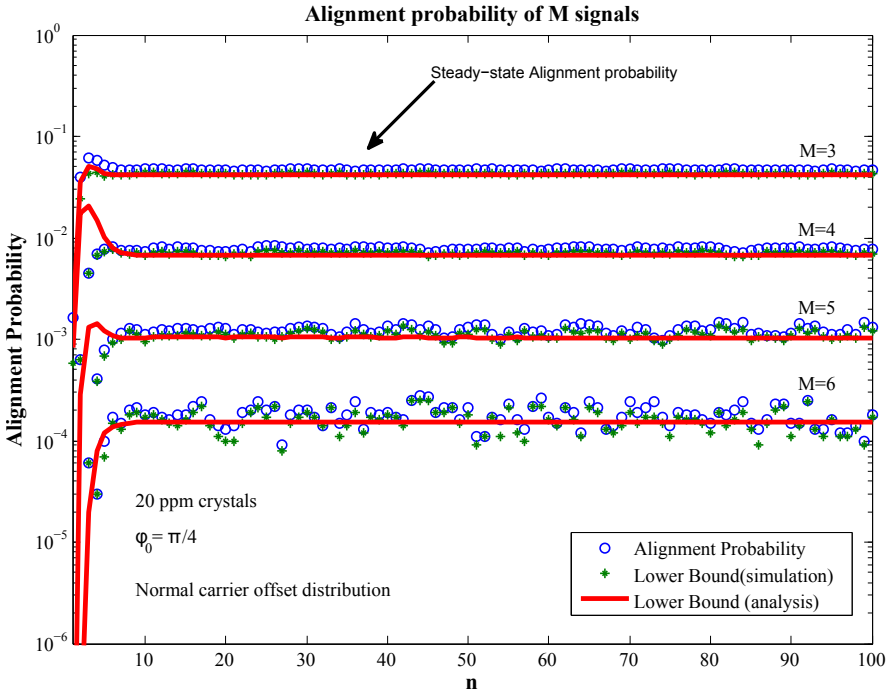

Figure 2.2: Alignment probability vs time (symbol number n).

test is given by:

$$\begin{aligned} H_0 &: \mathbf{y} = \mathbf{w}, \\ H_1 &: \mathbf{y} = \mathbf{g}x_1 + \mathbf{w}, \end{aligned} \tag{2.2}$$

where $\mathbf{g} = \begin{bmatrix} g_1 & \cdots & g_l & \cdots & g_L \end{bmatrix}^T$ and $\mathbf{w} = \begin{bmatrix} w_1 & \cdots & w_l & \cdots & w_L \end{bmatrix}^T$. The random variable $g_l \triangleq \sum_{m=1}^{M} h_m e^{+j2\pi\Delta f_m l T_s}$, for $l \in \{1, 2, \ldots, L\}$, is proved to be distributed according to $\mathcal{CN}(0, M)$ (see Appendix B.1-Lemma 1). The noise vector elements are i.i.d. according to $w_l \sim \mathcal{CN}(0, \sigma^2)$ for $l \in \{1, \ldots, L\}$.

2.3 Heuristic receiver

The time slots, where an alignment event can be occured, are not predictable. For this reason, a detector that considers only a subset of the slots cannot be

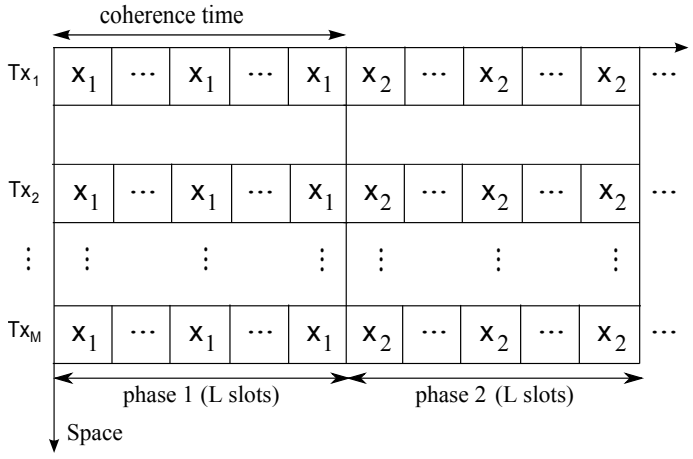

Figure 2.3: Repetitive transmission scheme. The M distributed transmitters simultaneously transmit the same information symbol for L slots, while the channel parameters remain unchanged.

used. Instead, all L symbols must be taken into account for detection, using energy detection technique:

$$\mathbf{y}^{\dagger}\mathbf{y} = \sum_{l=1}^{L} |y_l|^2. \tag{2.3}$$

Under H_0, the squared $\mathcal{L}_2$ norm of $\mathbf{y}$ is a Gamma-distributed random variable, as a sum of i.i.d. exponentials:

$$H_0 : \mathbf{y}^{\dagger}\mathbf{y} = \sum_{l=1}^{L} |w_l|^2 = w \sim \mathcal{G}\left(L, \sigma^2\right). \tag{2.4}$$

Under H_1 and given $\{\Delta f_m\}_{m\in\mathcal{T}}$, the squared $\mathcal{L}_2$ norm of $\mathbf{y}$, is a sum of correlated, identically Gamma-distributed random variables, i.e.,

$$H_1|\{\Delta f_m\}_{m\in\mathcal{T}} : \mathbf{y}^{\dagger}\mathbf{y} = \sum_{l=1}^{L} |y_l|^2 = \sum_{l=1}^{L} \zeta_l,\ \zeta_l \sim \mathcal{G}\left(1, Mx_1^2 + \sigma^2\right), \tag{2.5}$$

and ρ_{ij} is the correlation coefficient between ζ_i and ζ_j

$$\begin{aligned}\rho_{ij} &= \frac{\operatorname{cov}[\zeta_i, \zeta_j]}{\sqrt{\operatorname{var}[\zeta_i]\ \operatorname{var}[\zeta_j]}},\ i \neq j,\ i, j \in \{1, 2, \ldots, L\} \\ &= \frac{x_1^4 \Big\{ M + 2\sum_{k \neq n} \cos\left[2\pi T_s (\Delta f_k - \Delta f_n)(i-j)\right] \Big\}}{\left(M x_1^2 + \sigma^2\right)^2}. \end{aligned} \tag{2.6}$$

The sum in the ρ_{ij} calculation above is performed over all $\binom{M}{2}$ possible CFO pairs $(\Delta f_k, \Delta f_n)$.

A closed form for the p.d.f. of the sum of correlated Gamma is provided in [29, Eq. 5] while in [30], is offered as a function of the $L \times L$ matrix $\mathbf{K}$,

$$\mathbf{K} = \begin{bmatrix} 1 & \sqrt{\rho_{12}} & \cdots & \sqrt{\rho_{1L}} \\ \sqrt{\rho_{21}} & 1 & \cdots & \sqrt{\rho_{2L}} \\ \vdots & & & \cdots \\ \sqrt{\rho_{L1}} & \sqrt{\rho_{L2}} & \cdots & 1 \end{bmatrix} \tag{2.7}$$

for the special case where $\mathbf{K}$ is positive definite and $\rho_{ij} > 0$. In our problem, $\mathbf{K}$ is not necessarily positive definite, ρ_{ij} may be negative and thus, relevant analytical results in [29], [30] are not applicable in this work. For example, consider the case where $M = 2, L = 6$, $[\Delta f_1\ \Delta f_2] = [-0.6479e5\ 1.4568e5]$, then

$$\mathbf{K} = \begin{bmatrix} 1.0000 & 0.6863 & 0.2138 & 0.3489 & 0.7645 & 0.8578 \\ 0.6863 & 1.0000 & 0.6863 & 0.2138 & 0.3489 & 0.7645 \\ 0.2138 & 0.6863 & 1.0000 & 0.6863 & 0.2138 & 0.3489 \\ 0.3489 & 0.2138 & 0.6863 & 1.0000 & 0.6863 & 0.2138 \\ 0.7645 & 0.3489 & 0.2138 & 0.6863 & 1.0000 & 0.6863 \\ 0.8578 & 0.7645 & 0.3489 & 0.2138 & 0.6863 & 1.0000 \end{bmatrix}.$$

Its eigenvalues are

$$[-0.0449\ 0.0481\ 0.1444\ 1.0075\ 1.2311\ 3.6138]$$

and thus, $\mathbf{K}$ is not positive definite.
According to the above analysis, the statistics of $\mathbf{y}^{\dagger}\mathbf{y}$ are not known. Thus, assuming equiprobable symbols, a maximum-likelihood detector cannot be applied and an optimal threshold cannot be derived. Instead, a suboptimal method is used based on known statistics of $\mathbf{y}^{\dagger}\mathbf{y}$ under H_0.
The non-coherent detector is given by the following expression:

$$\mathbf{y}^{\dagger}\mathbf{y} = \sum_{l=1}^{L} |y_l|^2 \overset{H_1}{\geq} \theta_1(k). \tag{2.8}$$

The threshold $\theta_1(k)$ is appropriately selected in order to minimize the probability of false alarm ($P_{FA} = P(e \mid H_0)$). This error happens when the detector decides that $x_1 = \sqrt{E_1}$ was transmitted instead of $x_0 = 0$. Such case will occur when the sum of received samples contains large noise values are detected as constructive addition of transmitted signals. Thus, the threshold should be sufficiently large in order to minimize P_{FA}. The threshold is analytically expressed as:

$$\theta_1(k) = \mathbb{E}[w] + k\sqrt{\mathrm{var}[w]} = \sigma^2\left[L + k\sqrt{L}\right], k \in \mathbb{N} - \{0\}. \tag{2.9}$$

With the increment of k, the threshold based on first and second order statistics of $\mathbf{y}\mathbf{y}^{\dagger}$ under H_0 can be as large as we want. This implies that k parameter considers the Gamma distribution positive skewness, since the increment of k approximates better the maximum value of w follows the Gamma distribution tail. Hence, given a constraint ϵ on P_{FA}, the parameter k is analytically upper bounded:

$$\begin{aligned} P_{FA} \leq \epsilon &\Leftrightarrow \int_{\theta_1(k)}^{+\infty} \frac{1}{(\sigma^2)^L}\frac{1}{(L-1)!}x^{L-1}e^{-\frac{x}{\sigma^2}}dx \leq \epsilon \\ &\Leftrightarrow \frac{1}{(L-1)!}\Gamma\left(L, \frac{\theta_1(k)}{\sigma^2}\right) \leq \epsilon, \end{aligned} \tag{2.10}$$

where i.e., $\epsilon = 10^{-6}$ and $\Gamma(a,z) = \Gamma(a) - \gamma(a,z) = \int_z^{+\infty} t^{a-1}e^{-t}dt; \Re(a) > 0$, $\gamma(a,z)$ is the incomplete Gamma function [31, p. 260, Eq. 6.5.2] and $\Gamma(a)$ is the Gamma function [31, p. 255, Eq. 6.1.1]. Finally, the suboptimal k

parameter value selection is based on the overall BER minimization through simulations, since $P(e \mid H_1)$ must be also taken into account.

2.4 Equivalent channel taps

The equivalent channel taps[4] $\widetilde{\mathbf{g}}$ are defined as $\widetilde{\mathbf{g}} \triangleq \sqrt{\frac{1}{M}}\mathbf{g}$, where for $l \in \{1, 2, \ldots, L\}$, $\widetilde{\mathbf{g}} = \begin{bmatrix} \widetilde{g}_1 & \cdots & \widetilde{g}_l & \cdots & \widetilde{g}_L \end{bmatrix}^T$ and rv $\widetilde{g}_l = \sqrt{\frac{1}{M}} \sum_{m=1}^{M} h_m e^{+j2\pi\Delta f_m l T_s}$ is distributed according to $\mathcal{CN}(0, 1)$.

The correlation among the elements of vector $\widetilde{\mathbf{g}}$, $\{\widetilde{g}_l\}_{l=1}^{L}$, is described via a covariance matrix $\mathbf{C}$ where its analytical closed form is provided by the following theorem.

Theorem 1. *The covariance matrix of equivalent channel taps is given by:*

$$\mathbf{C} = \mathbb{E}\left[\widetilde{\mathbf{g}}\widetilde{\mathbf{g}}^{\dagger}\right] = \begin{bmatrix} 1 & \cdots & e^{-2\left[\pi(1-L)\sigma_f T_s\right]^2} \\ \vdots & \ddots & \vdots \\ e^{-2\left[\pi(L-1)\sigma_f T_s\right]^2} & \cdots & 1 \end{bmatrix}. \tag{2.11}$$

Proof. The random variables $\{\widetilde{g}_l\}_{l=1}^{L}$ are correlated and their $L \times L$ covariance matrix is expressed as $\mathbf{C} = \mathbb{E}\left[\widetilde{\mathbf{g}}\widetilde{\mathbf{g}}^{\dagger}\right]$. The $(k, l)^{\text{th}}$ element of covariance matrix $\mathbf{C}$, for $k, l \in \{1, \cdots, L\}$, is analytically computed as follows:[5]

$$\begin{aligned} \mathbb{E}_{\mathbf{h},\mathbf{e}}\left[\widetilde{g}_k \widetilde{g}_l^*\right] &= \mathbb{E}_{\mathbf{h},\mathbf{e}}\left[\left(\sqrt{\frac{1}{M}}\sum_{m=1}^{M} h_m e^{+j2\pi\Delta f_m k T_s}\right)\left(\sqrt{\frac{1}{M}}\sum_{n=1}^{M} h_n e^{+j2\pi\Delta f_n l T_s}\right)^*\right] \\ &= \frac{1}{M}\sum_{m=1}^{M} \mathbb{E}_{\mathbf{h},\mathbf{e}}\left[|h_m|^2 e^{+j2\pi\Delta f_m (k-l) T_s}\right] \\ &\overset{\substack{h_m, \Delta f_m \\ \text{indep.}}}{=} \frac{1}{M}\sum_{m=1}^{M} \mathbb{E}_{h_m}\left[|h_m|^2\right] \mathbb{E}_{\Delta f_m}\left[e^{+j2\pi\Delta f_m (k-l) T_s}\right] \end{aligned}$$

[4] At this point and throughout this thesis, the term "equivalent channel taps" will stand for $\{\widetilde{g}_l\}_{l=1}^{L}$.

[5] For notational convenience, random vectors $\mathbf{h} \triangleq \begin{bmatrix} h_1 & \cdots & h_M \end{bmatrix}^T$ and $\mathbf{e} \triangleq \begin{bmatrix} \Delta f_1 & \cdots & \Delta f_M \end{bmatrix}^T$ are defined.

$$= \frac{1}{M\sqrt{2\pi\sigma_f^2}} \times \sum_{m=1}^{M} \int_{-\infty}^{+\infty} e^{\frac{+j4\pi\sigma_f^2\Delta f_m(k-l)T_s - \Delta f_m^2}{2\sigma_f^2}} d\Delta f_m. \tag{2.12}$$

The integral above in Eq. (2.12) is computed according to [32, p.163, Eq. 7.7.6]:

$$\begin{aligned} I &= \lim_{x\to-\infty} \left[\int_x^{+\infty} e^{\frac{+j4\pi\sigma_f^2\Delta f_m(k-l)T_s - \Delta f_m^2}{2\sigma_f^2}} d\Delta f_m \right] \\ &= \frac{1}{2}\sqrt{2\pi\sigma_f^2}\; e^{-2\left[\pi(k-l)\sigma_f T_s\right]^2} \times \lim_{x\to-\infty} \operatorname{erfc}\left(\sqrt{\frac{1}{2\sigma_f^2}} x - j\sqrt{2}\pi\,(k-l)\,\sigma_f T_s \right) \\ &= \sqrt{2\pi\sigma_f^2}\; e^{-2\left[\pi(k-l)\sigma_f T_s\right]^2}. \end{aligned} \tag{2.13}$$

From Eqs. (2.12), (2.13), the $(k,l)^{\text{th}}$ element of covariance matrix $\mathbf{C}$ becomes:

$$\mathbb{E}_{\mathbf{h},\mathbf{e}}\left[\widetilde{g}_k \widetilde{g}_l^*\right] = e^{-2\left[\pi(k-l)\sigma_f T_s\right]^2}, \tag{2.14}$$

and the matrix $\mathbf{C}$ is analytically described as:

$$\mathbf{C} = \mathbb{E}\left[\widetilde{\mathbf{g}}\widetilde{\mathbf{g}}^\dagger\right] = \begin{bmatrix} 1 & \cdots & e^{-2\left[\pi(1-L)\sigma_f T_s\right]^2} \\ \vdots & \ddots & \vdots \\ e^{-2\left[\pi(L-1)\sigma_f T_s\right]^2} & \cdots & 1 \end{bmatrix}. \tag{2.15}$$

□

Considering the exponential terms of matrix $\mathbf{C}$, it can be easily seen that the appropriate selection of parameters L, σ_f, T_s leads to different types of correlation. In other words, the correlation coefficient of $\{\widetilde{g}_l\}_{l=1}^{L}$, $\rho_{\widetilde{g}_k,\widetilde{g}_l} = \frac{\mathbb{E}\left\{\widetilde{g}_k \widetilde{g}_l^*\right\}}{\sigma_{\widetilde{g}_k}\sigma_{\widetilde{g}_l}} = e^{-2\left[\pi(k-l)\sigma_f T_s\right]^2}$, $\forall\ k \neq l,\ k,l \in \{1,\ \ldots,\ L\}$, is a function of these parameters. According to the value of $0 \leq \rho_{\widetilde{g}_k,\widetilde{g}_l} \leq 1$, equivalent channel taps are fully-correlated ($\rho_{\widetilde{g}_k,\widetilde{g}_l} = 1$), partially correlated ($0 < \rho_{\widetilde{g}_k,\widetilde{g}_l} < 1$) or uncorrelated ($\rho_{\widetilde{g}_k,\widetilde{g}_l} = 0$).

2.5 ZF-DBF receiver for fully-correlated equivalent channel taps

Theorem 2. *The random vector* $\mathbf{g}$ *is distributed according to* $\mathcal{CN}\left(\mathbf{0}, \boldsymbol{\alpha}\boldsymbol{\alpha}^{\dagger}M\right)$*, where* $\boldsymbol{\alpha} = \begin{bmatrix} 1 & \cdots & 1 \end{bmatrix}^{T}$*, if the elements of vector* $\widetilde{\mathbf{g}} = \sqrt{\frac{1}{M}}\mathbf{g}$ *are fully correlated (in the sense of* $e^{-2\left[\pi(k-l)\sigma_f T_s\right]^2} \simeq 1$*).*

Proof. The $(k,l)^{\text{th}}$ element of matrix $\mathbf{C}$, $e^{-2\left[\pi(k-l)\sigma_f T_s\right]^2} \simeq 1$, for $k \neq l$, if the exponent $-2\left[\pi\left(k-l\right)\sigma_f T_s\right]^2 \simeq 0$. This happens with appropriate selection of parameters σ_f, T_s, L in order to satisfy the condition $L{\cdot}\sigma_f{\cdot}T_s \simeq 0$. The square included in the exponent accelerates convergence of the exponential term to unity, when the sufficient condition $L \cdot \sigma_f \cdot T_s \simeq 0$ holds. For instance, if $\sigma_f = 2.4\,\text{GHz}{\times}2\,\text{ppm} = 4.8\,\text{kHz}$, $T_s = 1\,\mu s$ and $L = 4$, then $e^{-2\left[\pi(k-l)\sigma_f T_s\right]^2} \simeq 1$, for $k \neq l$. This is a frequent case, assuming high transmission rate in RF bands and a typical value of ppm ($\times 10^{-6}$), where small L is selected for repetitive transmission in order to avoid rate degradation. This case implies that all the elements of random vector $\widetilde{\mathbf{g}}$ are fully correlated (in the sense of $e^{-2\left[\pi(k-l)\sigma_f T_s\right]^2} \simeq 1$), since their correlation coefficient $\rho_{\widetilde{g}_k,\widetilde{g}_l} \simeq 1$, $\forall\ k \neq l,\ k,l \in \{1,\ \ldots,\ L\}$. In this case, the random vector $\widetilde{\mathbf{g}}$ can be replaced by the random vector $\boldsymbol{\alpha}g_0 \sim \mathcal{CN}\left(\mathbf{0}, \boldsymbol{\alpha}\boldsymbol{\alpha}^{\dagger}\right)$, where $g_0 \sim \mathcal{CN}\left(0,1\right)$ and $\boldsymbol{\alpha} = \begin{bmatrix} 1 & \cdots & 1 \end{bmatrix}^{T}$. Exploiting the above, it can be directly concluded that $\mathbf{g} \sim \mathcal{CN}\left(\mathbf{0}, \boldsymbol{\alpha}\boldsymbol{\alpha}^{\dagger}M\right)$. □

2.5.1 Maximum-likelihood non-coherent detector

The maximum-likelihood detector derived in this subsection is referred only to the fully-correlated *equivalent channel taps* case. Using Theorem 2, under $H_1 : \mathbf{y} \sim \mathcal{CN}\left(\mathbf{0}, \boldsymbol{\alpha}\boldsymbol{\alpha}^{\dagger}Mx_1^2 + \sigma^2\mathbf{I}_L\right)$ as an affine transformation of independent circularly-symmetric complex Gaussian random vectors and under $H_0 : \mathbf{y} \sim \mathcal{CN}\left(\mathbf{0}, \sigma^2\mathbf{I}_L\right)$. Applying MAP and assuming equiprobable symbols,

we conclude to our ML non-coherent detector:

$$\begin{aligned}\hat{H}_i \text{ such that } i &= \arg \max_{j\in\{0,1\}} P\left(H_j \mid \mathbf{y}\right) \\ &= \arg \max_{j\in\{0,1\}} \frac{f_{\mathbf{y}|H_j}\left(\mathbf{y} \mid H_j\right)P\left(H_j\right)}{f_{\mathbf{y}}\left(\mathbf{y}\right)} \\ &= \arg \max_{j\in\{0,1\}} f_{\mathbf{y}|H_j}\left(\mathbf{y} \mid H_j\right).\end{aligned}$$

After simple calculations, the ML non-coherent detector is simplified to:

$$\begin{gathered} f_{\mathbf{y}|H_1}\left(\mathbf{y} \mid H_1\right) \overset{H_1}{\geq} f_{\mathbf{y}|H_0}\left(\mathbf{y} \mid H_0\right) \Leftrightarrow \\ \frac{\exp\left[-\mathbf{y}^\dagger\left(\boldsymbol{\alpha}\boldsymbol{\alpha}^\dagger M x_1^2 + \sigma^2\mathbf{I}_L\right)^{-1}\mathbf{y}\right]}{\pi^L \det\left(\boldsymbol{\alpha}\boldsymbol{\alpha}^\dagger M x_1^2 + \sigma^2\mathbf{I}_L\right)} \overset{H_1}{\geq} \frac{1}{(\pi\sigma^2)^L}\exp\left(-\frac{||\mathbf{y}||_2^2}{\sigma^2}\right) \Leftrightarrow \\ \mathbf{y}^\dagger\mathbf{D}\mathbf{y} \overset{H_1}{\geq} \theta_2 \triangleq \sigma^2 \ln\left[\det\left(\mathbf{I}_L + \boldsymbol{\alpha}\boldsymbol{\alpha}^\dagger\frac{Mx_1^2}{\sigma^2}\right)\right], \end{gathered} \tag{2.16}$$

where $\mathbf{D} \triangleq \mathbf{I}_L - \left(\mathbf{I}_L + \boldsymbol{\alpha}\boldsymbol{\alpha}^\dagger\frac{Mx_1^2}{\sigma^2}\right)^{-1}$.

2.5.2 BER performance analysis

Theorem 3. *Assuming fully-correlated equivalent channel taps and equiprobable hypotheses, the average BER for the ML non-coherent detector is given by:*

$$P\left(e\right) = \frac{1}{2}\left[1 - F_r\left(\boldsymbol{\lambda}_{H_0}, \theta_2\right) + F_r\left(\boldsymbol{\lambda}_{H_1}, \theta_2\right)\right], \tag{2.17}$$

where under hypothesis H_i, $i \in \{0,1\}$, $F_r\left(\boldsymbol{\lambda}_{H_i}, \theta_2\right)$ is the c.d.f. of $\mathbf{y}^\dagger\mathbf{D}\mathbf{y}$. Furthermore, analytical form of c.d.f. $F_r\left(\boldsymbol{\lambda}_{H_i}, \theta_2\right)$ is given in Appendix B.2. Vector $\boldsymbol{\lambda}_{H_i}$ contains the eigenvalues of a $2L \times 2L$ matrix $\left(\boldsymbol{\Sigma}_{H_i}\right)^{\frac{1}{2}}\mathbf{E}\left(\boldsymbol{\Sigma}_{H_i}\right)^{\frac{1}{2}}$ and $r = rank\left(\mathbf{E}\right)$.

$$\mathbf{E} = \begin{bmatrix} \mathbf{D} & 0_{L\times L} \\ 0_{L\times L} & \mathbf{D} \end{bmatrix},\ \boldsymbol{\Sigma}_{H_1} = \begin{bmatrix} \frac{1}{2}\left(\boldsymbol{\alpha}\boldsymbol{\alpha}^{\dagger}Mx_1^2 + \sigma^2\mathbf{I}_L\right) & 0_{L\times L} \\ 0_{L\times L} & \frac{1}{2}\left(\boldsymbol{\alpha}\boldsymbol{\alpha}^{\dagger}Mx_1^2 + \sigma^2\mathbf{I}_L\right) \end{bmatrix}$$

and $\boldsymbol{\Sigma}_{H_0} = \begin{bmatrix} \frac{1}{2}\sigma^2\mathbf{I}_L & 0_{L\times L} \\ 0_{L\times L} & \frac{1}{2}\sigma^2\mathbf{I}_L \end{bmatrix}$.

Proof. Assuming equiprobable hypotheses, BER is written as:

$$\begin{aligned} P(e) &= \sum_{i=0}^{1} P(e \mid H_i)P(H_i) \\ &= \frac{1}{2}\left[P(\mathbf{y}^{\dagger}\mathbf{D}\mathbf{y} \geq \theta_2 \mid H_0) + P(\mathbf{y}^{\dagger}\mathbf{D}\mathbf{y} < \theta_2 \mid H_1)\right] \\ &= \frac{1}{2}\left[1 - F_r\left(\boldsymbol{\lambda}_{H_0}, \theta_2\right) + F_r\left(\boldsymbol{\lambda}_{H_1}, \theta_2\right)\right], \end{aligned} \tag{2.18}$$

where $P(e \mid H_i)$ for $i = 0, 1$ are calculated by the c.d.f. of $\mathbf{y}^{\dagger}\mathbf{D}\mathbf{y}$ described in Appendix B.2-Eq. (B.3). □

2.6 ZF-DBF receiver for not fully-correlated equivalent channel taps

For the case of not fully-correlated equivalent channel taps $\{\widetilde{g}_l\}_{l=1}^{L}$, the p.d.f. of $\mathbf{g}$ is not known. Given $\{\Delta f_m\}_{m\in\mathcal{T}}$, the random vector $\mathbf{g}$ can be written as $\mathbf{g} = \mathbf{A}\mathbf{h}$ and is distributed according to the conditional p.d.f. $f_{\mathbf{g}|\mathbf{A}}(\mathbf{g} \mid \mathbf{A}) = f_{\mathbf{g}|\{\Delta f_m\}_{m\in\mathcal{T}}}\left(\mathbf{g} \mid \{\Delta f_m\}_{m\in\mathcal{T}}\right) \equiv \mathcal{CN}\left(\mathbf{0}, \mathbf{A}\mathbf{A}^{\dagger}\right)$, as a linear combination of a circularly-symmetric complex Gaussian vector $\mathbf{h} = \begin{bmatrix} h_1 & h_2 & \dots & h_M \end{bmatrix}^T \sim \mathcal{CN}(\mathbf{0}, \mathbf{I}_M)$, where $L \times L$ matrix $\mathbf{A}$ is expressed as:

$$\mathbf{A} = \begin{bmatrix} e^{+j2\pi\Delta f_1 T_s} & \dots & e^{+j2\pi\Delta f_M T_s} \\ \vdots & \ddots & \vdots \\ e^{+j2\pi\Delta f_1 LT_s} & \dots & e^{+j2\pi\Delta f_M LT_s} \end{bmatrix}. \tag{2.19}$$

However, the p.d.f. of $\mathbf{A}$ is not known, and thus, a closed form for the unconditioned p.d.f. of $\mathbf{g}$ cannot be derived. Therefore, for partially correlated and uncorrelated equivalent channel taps, a heuristic receiver is proposed by replacing the term $\boldsymbol{\alpha}\boldsymbol{\alpha}^{\dagger}$ of Eq. (3.3) with $\mathbf{C}$:

$$\mathbf{y}^{\dagger}\mathbf{G}\mathbf{y} \overset{H_1}{\geq} \theta_3 \triangleq \sigma^2 \ln\left[\det\left(\mathbf{I}_L + \mathbf{C}\frac{Mx_1^2}{\sigma^2}\right)\right], \tag{2.20}$$

where $\mathbf{C}$ is given by Eq. (2.15) and $\mathbf{G} \triangleq \mathbf{I}_L - \left(\mathbf{I}_L + \mathbf{C}\frac{Mx_1^2}{\sigma^2}\right)^{-1}$.

Chapter 3

Energy harvesting TDMA receiver

In this chapter, a protocol based on energy harvesting at receiver is presented. The distributed terminals are power constrained according to the system assumptions, thus the received energy of each node is limited. A way to increase your received energy is to collect replicates of the same information symbol in time via a TDMA protocol among the distributed nodes for ensuring reliable connectivity in terms of BER. A non-coherent maximum-likelihood receiver is proposed for this scheme and its BER performance in close form is enclosed.

3.1 Transmission Protocol

Transmission of the same symbol using time-division multiplexing via M distributed terminals is performed for L slots (one phase). Each commodity radio transmits independently from the others the same symbol for $[L/M]$ slots. In that way, the receiver increases the received energy, in order to achieve reliable detection at the expense of rate. If M does not divide L ($M \nmid L$), the remaining slots are allocated to the j^{th} terminal, $j \in \{1, \cdots, M\}$, that is selected randomly (uniformly) (Fig. 3.1). Hence, if M divides L ($M \mid L$), then $j = 0$, since no one extra user is needed to transmit. Additionally, the achieved rate is $1/L$, the same as in ZF-DBF transmission protocol. Assuming CFO correction at the receiver, the signal model is expressed as:

$$\mathbf{y} = \widetilde{\mathbf{h}}x + \mathbf{w}, \tag{3.1}$$

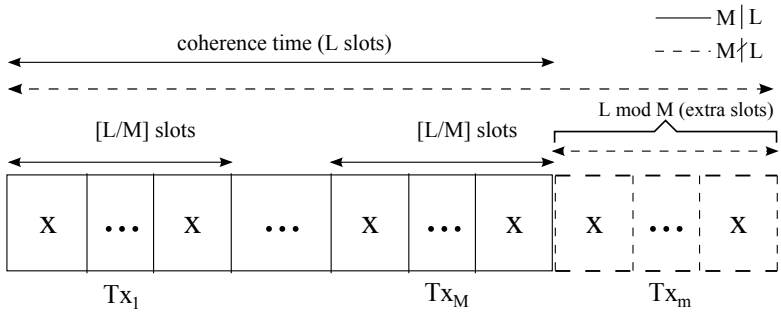

Figure 3.1: Non-coherent energy harvesting (TDMA) scheme.

where

$$\widetilde{\mathbf{h}} \triangleq \begin{cases} \left[\underbrace{h_1 \cdots h_1}_{[L/M]} \quad \cdots \quad \underbrace{h_M \cdots h_M}_{[L/M]}\right]^T & \text{, if } M \mid L. \\ \left[\underbrace{h_1 \cdots h_1}_{[L/M]} \quad \cdots \quad \underbrace{h_M \cdots h_M}_{[L/M]} \quad \underbrace{h_m \cdots h_m}_{L \mod M}\right]^T & \text{, if } M \nmid L. \end{cases}$$

Finally, the random variable $h_m \sim \mathcal{CN}(0,1), m \in \{1,\ldots,M\}$ and $\mathbf{w} \sim \mathcal{CN}(\mathbf{0}, \mathbf{I}_L)$.

3.2 Maximum-likelihood non-coherent detector

Given the hypotheses, Eq. (3.1) can be written as:

$$\begin{aligned} H_0 &: \mathbf{y} = \mathbf{w}, \\ H_1 &: \mathbf{y} = \mathbf{B}_j \mathbf{h} x_1 + \mathbf{w}, \end{aligned} \tag{3.2}$$

where

$$\mathbf{B}_j = \begin{bmatrix} 1 & 0 & \cdots & 0 & 0 \\ & & \vdots & & \\ 1 & 0 & \cdots & 0 & 0 \\ 0 & 1 & \cdots & 0 & 0 \\ & & \vdots & & \\ 0 & 1 & \cdots & 0 & 0 \\ & & \vdots & & \\ 0 & 0 & \cdots & 0 & 1 \\ & & \vdots & & \\ 0 & 0 & \cdots & 0 & 1 \\ & \text{extra rows} & & & \end{bmatrix} \begin{matrix} \\ \\ \left[\frac{L}{M}\right] \text{ rows } (1^{\text{st}} \text{ user block}) \\ \\ \left[\frac{L}{M}\right] \text{ rows } (2^{\text{nd}} \text{ user block}) \\ \\ \left[\frac{L}{M}\right] \text{ rows } (M^{\text{th}} \text{ user block}) \\ \\ L \mod M \text{ rows (extra } j^{\text{th}} \text{ user block)}, \end{matrix}$$

$$\mathbf{h} = \begin{bmatrix} h_1 & h_2 & \cdots & h_M \end{bmatrix}^T \sim \mathcal{CN}(\mathbf{0}, \mathbf{I}_M) \text{ and } j \in \begin{cases} \{0\} & , \text{ if } M \mid L \\ \{1, \cdots, M\} & , \text{ if } M \nmid L \end{cases}.$$

Each block of $[L/M]$ rows of matrix $\mathbf{B}_j$ corresponds to the m^{th} user transmission. The extra rows of matrix $\mathbf{B}_j$ are selected to be the same with one of the $[L/M]$ rows of the j^{th} user block. Thus, the extra rows correspond to a different j^{th} user which is selected uniformly. Finally, if $M \nmid L$, then $j \neq 0$, since an extra user is needed to transmit and if $M \mid L$, then $j = 0$, since no one extra user is needed.

Under $H_1: \ \mathbf{y} \sim \mathcal{CN}\left(\mathbf{0}, \mathbf{B}_j \mathbf{B}_j^\dagger x_1^2 + \sigma^2 \mathbf{I}_L\right)$ as an affine transformation of independent circularly-symmetric complex Gaussian random vectors and under $H_0: \ \mathbf{y} \sim \mathcal{CN}(\mathbf{0}, \sigma^2 \mathbf{I}_L)$.

Assuming equiprobable symbols, ML non-coherent is:

$$f_{\mathbf{y}|H_1}(\mathbf{y} \mid H_1) \overset{H_1}{\geq} f_{\mathbf{y}|H_0}(\mathbf{y} \mid H_0) \Leftrightarrow$$

$$\frac{\exp\left[-\mathbf{y}^\dagger \left(\mathbf{B}_j \mathbf{B}_j^\dagger x_1^2 + \sigma^2 \mathbf{I}_L\right)^{-1} \mathbf{y}\right]}{\pi^L \det\left(\mathbf{B}_j \mathbf{B}_j^\dagger x_1^2 + \sigma^2 \mathbf{I}_L\right)} \overset{H_1}{\geq} \frac{1}{(\pi\sigma^2)^L} \exp\left(-\frac{||\mathbf{y}||_2^2}{\sigma^2}\right) \Leftrightarrow$$

$$\mathbf{y}^{\dagger}\mathbf{R}_j\mathbf{y} \overset{H_1}{\geq} \Theta \triangleq \sigma^2 \ln\left[\det\left(\mathbf{I}_L + \mathbf{B}_j\mathbf{B}_j^{\dagger}\frac{x_1^2}{\sigma^2}\right)\right], \tag{3.3}$$

where $\mathbf{R}_j \triangleq \mathbf{I}_L - \left(\mathbf{I}_L + \mathbf{B}_j\mathbf{B}_j^{\dagger}\frac{x_1^2}{\sigma^2}\right)^{-1}$.

3.3 BER performance analysis

Similarly to the methodology of subsection 2.5.2, the c.d.f. of complex quadratic form $\mathbf{y}^{\dagger}\mathbf{R}_j\mathbf{y}$ is needed to describe the probability of error under each hypothesis. The theorem below provides BER analysis of the TDMA receiver both for the case of $M \mid L$ and $M \nmid L$.

Theorem 4. *Assuming equiprobable symbols, BER closed form both for the cases of $M \mid L$ and $M \nmid L$ is given by:*

$$P(e) = \begin{cases} \frac{1}{2}\left[1 - F_r\left(\boldsymbol{\lambda}_{H_0}^0, \Theta\right) + F_r\left(\boldsymbol{\lambda}_{H_1}^0, \Theta\right)\right] & , \text{ if } M \mid L, \\ \\ \frac{1}{2M}\sum_{j=1}^{M}\left[1 - F_r\left(\boldsymbol{\lambda}_{H_0}^j, \Theta\right) + F_r\left(\boldsymbol{\lambda}_{H_1}^j, \Theta\right)\right] & , \text{ if } M \nmid L, \end{cases} \tag{3.4}$$

where $F_r(\cdot,\cdot)$ is, the c.d.f. of $\mathbf{y}^{\dagger}\mathbf{R}_j\mathbf{y}$ (given at the Appendix B.2).

$$\mathbf{E}_j = \begin{bmatrix} \mathbf{R}_j & 0_{L\times L} \\ \\ 0_{L\times L} & \mathbf{R}_j \end{bmatrix}, \ \boldsymbol{\Sigma}_{H_1} = \begin{bmatrix} \frac{1}{2}\left(\mathbf{B}_j\mathbf{B}_j^{\dagger}x_1^2 + \sigma^2\mathbf{I}_L\right) & 0_{L\times L} \\ \\ 0_{L\times L} & \frac{1}{2}\left(\mathbf{B}_j\mathbf{B}_j^{\dagger}x_1^2 + \sigma^2\mathbf{I}_L\right) \end{bmatrix}$$

and $\boldsymbol{\Sigma}_{H_0} = \begin{bmatrix} \frac{1}{2}\sigma^2\mathbf{I}_L & 0_{L\times L} \\ \\ 0_{L\times L} & \frac{1}{2}\sigma^2\mathbf{I}_L \end{bmatrix}$.

Under H_i, $i \in \{0,1\}$, vectors $\boldsymbol{\lambda}_{H_i}^0$ (case for $M \mid L$) and $\boldsymbol{\lambda}_{H_i}^j$ (case for $M \nmid L$) contain the eigenvalues of the $2L \times 2L$ matrix $\left(\boldsymbol{\Sigma}_{H_i}\right)^{\frac{1}{2}}\mathbf{E}_j\left(\boldsymbol{\Sigma}_{H_i}\right)^{\frac{1}{2}}$, where for the case of $M \mid L$, matrix $\mathbf{E}_0$ is based on $\mathbf{R}_0$ constructed by $\mathbf{B}_0$ without including any extra rows and for the case of $M \nmid L$, matrix $\mathbf{E}_j$ is based on $\mathbf{R}_j$ constructed by $\mathbf{B}_j$ with extra rows (i.e., the $L \mod M$ rows of the j^{th} user block). Finally, $r = rank(\mathbf{E}_j)$.

Proof. Considering the cases of $M \mid L$ and $M \nmid L$, the analysis follows as:

If $M \mid L$, BER is computed as:

$$\begin{aligned} P(e) &= \sum_{i=0}^{1} P(e \mid H_i) P(H_i) = \frac{1}{2} \sum_{i=0}^{1} P(e \mid H_i) \\ &= \frac{1}{2} \left[P(\mathbf{y}^\dagger \mathbf{R}_0 \mathbf{y} \geq \Theta \mid H_0) + P(\mathbf{y}^\dagger \mathbf{R}_0 \mathbf{y} < \Theta \mid H_1) \right] \\ &= \frac{1}{2} \left[1 - F_r \left(\boldsymbol{\lambda}_{H_0}^0, \Theta \right) + F_r \left(\boldsymbol{\lambda}_{H_1}^0, \Theta \right) \right]. \end{aligned} \tag{3.5}$$

If $M \nmid L$, BER is computed as:

$$\begin{aligned} P(e) &= \frac{1}{2} \sum_{i=0}^{1} P(e \mid H_i) = \frac{1}{2} \sum_{j=1}^{M} \sum_{i=0}^{1} P(e \cap Tx_j \mid H_i) \\ &= \frac{1}{2} \sum_{j=1}^{M} \sum_{i=0}^{1} P(e \mid \mathrm{Tx}_j, H_i) \underbrace{P(\mathrm{Tx}_j \mid H_i)}_{P(\mathrm{Tx}_j)}, \end{aligned} \tag{3.6}$$

where Tx_j denotes the event of the j^{th} user transmission at the extra allocated slots. Since, the extra slots are allocated uniformly, the probability $P(\mathrm{Tx}_j)$ is set to $P(\mathrm{Tx}_j) = \frac{1}{M}$. Consequently, Eq. (3.6) becomes:

$$\begin{aligned} P(e) &= \frac{1}{2M} \sum_{j=1}^{M} \sum_{i=0}^{1} P(e \mid \mathrm{Tx}_j, H_i) \\ &= \frac{1}{2M} \sum_{j=1}^{M} \left[P(e \mid \mathrm{Tx}_j, H_0) + P(e \mid \mathrm{Tx}_j, H_1) \right] \\ &= \frac{1}{2M} \sum_{j=1}^{M} \left[P(\mathbf{y}^\dagger \mathbf{R}_j \mathbf{y} \geq \Theta \mid \mathrm{Tx}_j, H_0) + P(\mathbf{y}^\dagger \mathbf{R}_j \mathbf{y} < \Theta \mid \mathrm{Tx}_j, H_1) \right] \\ &= \frac{1}{2M} \sum_{j=1}^{M} \left[1 - F_r \left(\boldsymbol{\lambda}_{H_0}^j, \Theta \right) + F_r \left(\boldsymbol{\lambda}_{H_1}^j, \Theta \right) \right]. \end{aligned} \tag{3.7}$$

Using the derived closed form c.d.f of of $\mathbf{y}^\dagger \mathbf{R}_j \mathbf{y}$, as described in Appendix B.2-Eq. (B.3), under each hypothesis and given the j^{th} user transmission (implying $\mathbf{R}_j$ construction with extra rows in $\mathbf{B}_j$, the $L \mod M$ rows of the

j^{th} user block, if $M \nmid L$ or no extra rows ($j = 0$) if $M \mid L$, Eq. (3.5) and Eq. (3.7) result in Eq. (3.4).

Parameter r is the same for the cases of $M \mid L$ and $M \nmid L$, since for the case of $M \nmid L$, the addition of extra rows in matrix $\mathbf{B}_j$ leaves the rank of matrix $\mathbf{B}_j$ unchanged and thus the rank of matrix $\mathbf{R}_j$ is also the same. $\square$

Chapter 4

Evaluation and numerical results

This chapter presents numerical and analytical results on the proposed non-coherent receivers for the ZF-DBF and TDMA schemes. The assumptions of the system include low-cost power constrained transmitters, thus this work focuses on low-SNR regime where reliable connectivity seems to be infeasible. The presented results show that collaborative schemes can perform better than one single node transmission. ZF-DBF scheme provides beamforming gain alleviating network partitioning problems in low SNR regimes at the expense of power and rate degradation. Hence, nodes transmitting in a round-robin fashion using a TDMA scheme can offer diversity using the independence of users' channels for high SNR regimes.

4.1 ZF-DBF receivers vs Energy harvesting TDMA receiver

Both numerical and analytical results are presented with SNR per transmitter antenna per time slot, as defined in Eq. (1.2). All the proposed schemes operates at the same power per transmitter antenna per time slot and assume that this is the maximum power offered by the low-cost commodity radios. Furthermore, the distributed terminals are assumed to operate at $f_c = 2.4$ GHz and the L parameter is selected to be small ($L = 3, 4$) so as not to degrade a lot the achieved rate $1/L$, both for the ZF-DBF and energy harvesting TDMA schemes.

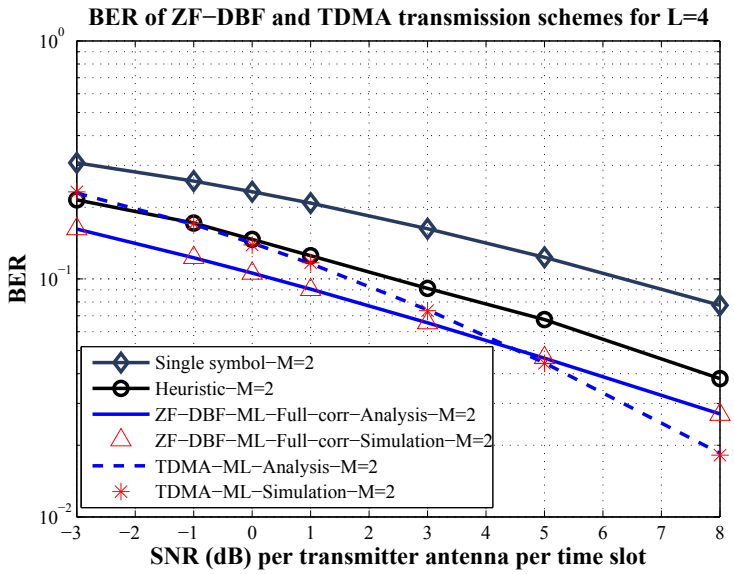

Figure 4.1: BER performance for ZF-DBF and TDMA transmission schemes (L=4).

4.1.1 Fully-correlated channel taps

In this subsection analytical and numerical results for fully-correlated equivalent channel taps are presented. In this case, the condition $L \cdot \sigma_f \cdot T_s \simeq 0$ must be satisfied, thus $\sigma_f = f_c \times$ ppm, T_s and L are appropriately selected in order to adhere this condition. For the presented results, 2 ppm clock frequency skew and $T_s = 1\ \mu s$ (high transmission rate) were selected. For these values, the equivalent channel taps at the destination receiver are fully correlated and exploited in the appropriate detector (Figs. 4.1–4.4).

ZF-DBF and energy harvesting (TDMA) schemes BER curves are provided as a function of SNR per transmitter antenna per time slot. The depicted results are for $M = 2$ distributed transmitters and $L = 4$ symbols. Fully-correlated equivalent channel taps ML ZF-DBF receiver outperforms the heuristic receiver, as optimal in terms of BER. For SNR values up to 5 dB ML ZF-DBF for fully-correlated equivalent channel taps receiver is better than the TDMA one. ZF-DBF achieves better performance at lower SNR regimes due to the beamforming gain provided, at the expense of additional

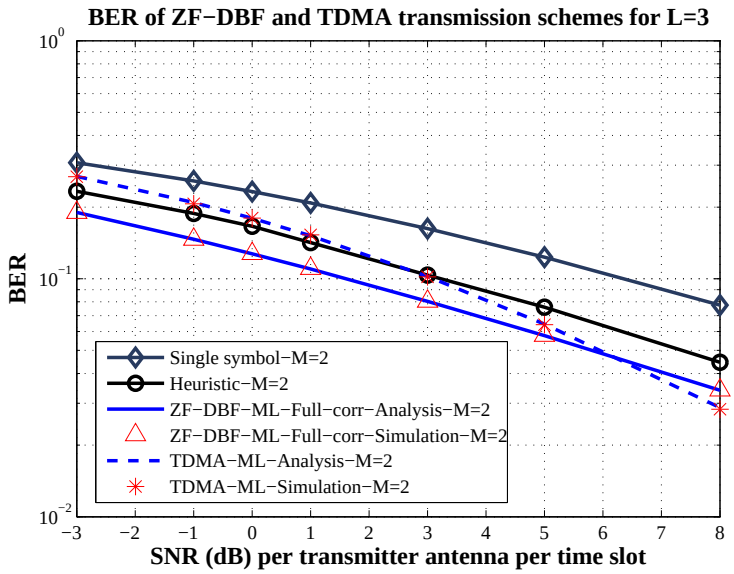

Figure 4.2: BER performance for ZF-DBF and TDMA transmission schemes (L=3).

transmission power consumption. Compared to TDMA, there is a factor of M. Hence, TDMA has better performance at high SNR regimes, since diversity exists from the M independent channel taps. BER performance for single symbol non-coherent detector (ZF-DBF ML detector of Eq. (3.3) for $L = 1$) is also presented for comparison purposes.

BER simulation and analytical results for the ZF-DBF and TDMA schemes, $M = 2$ distributed transmitters and smaller L value ($L = 3$ symbols) are depicted in Fig. 4.2. For ZF-DBF scheme, the expected number of symbols (out of L) can be easily computed via expression in [27, Eq. 12]. For instance, the case of $L = 4$ with $M = 2$ aligned signals within at most $\phi_0 = \pi/4$ gives expected number of symbols equals to 1. Thus, there is one slot on average with beamforming gain in $L = 4$ transmitted symbols. If $L = 3$, then the expected number of symbols is strictly smaller than 1. This implies that reducing L augments the achieved rate $1/L$, but BER performance is degraded due to there is no guarantee of an alignment event, as shown in the figure. For low SNR regimes (up to 6 dB), ZF-DBF outperforms the TDMA receiver. Furthermore, BER TDMA receiver performance is degraded for

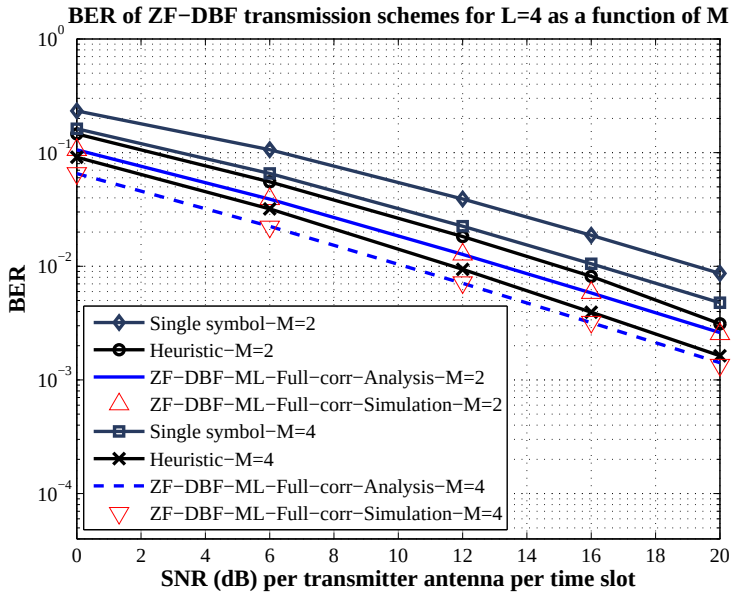

Figure 4.3: BER performance for ZF-DBF transmission schemes with different number of M distributed terminals.

$L = 3$ compared to the $L = 4$ case, since less number of time slots does not provide the same diversity. On the contrary, smaller L ameliorates the achieved rate. Consequently, there is a trade-off between better rate and smaller BER (trustworthy connectivity), especially at lower SNR regimes at the expense of additional transmission power. Nonetheless, exploiting the battery-operated distributed terminals in order to reach the destination in resource constrained networks, may be designer's only option.

Fig. 4.3 provides simulation and analytical results for the ZF-DBF scheme for $L = 4$ symbols and different number of M distributed terminals. As the number M of distributed terminals increases, the signal alignment probability decreases exponentially with M [27]; BER performance is getting better with the increment of M, thus again, there is a trade-off between total transmission power and reliable connectivity. In dust distributed low-cost wireless sensor networks, where one node is inadequate to reach the destination, zero-feedback beamforming can be exploited by distributed nodes offering their radios batteries.

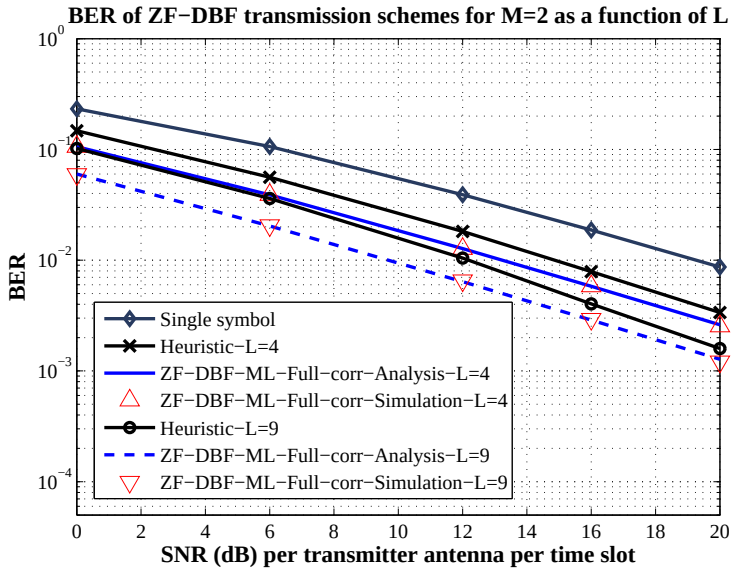

Figure 4.4: BER performance for ZF-DBF transmission schemes in different L time intervals.

Fig. 4.4 offers BER performance for the ZF-DBF scheme for a different number of L symbols and $M = 2$ terminals. As figure depicts, BER performance is improved with the increment of parameter L, since repetitive transmission period is expanded, offering reliability, at the expense of total power consumption and rate degradation.

4.1.2 Not fully-correlated channel taps

This subsection provides analysis and simulation results for different types of correlation among the equivalent channel taps. Fully-correlated case was examined with 2 ppm and $T_s = 1\ \mu s$. These values lead to an all-ones $\mathbf{C}$ matrix (see Eq. (2.15)), implying full-correlation. Selecting different values for ppm and T_s, $\mathbf{C}$ matrix is completely changed and consequently the correlation type of equivalent channel taps. Both partially correlated equivalent channel taps with $T_s = 1\ \mu s$, 20 ppm clock crystals and uncorrelated equivalent channel taps with $T_s = 0.4$ ms, 2 ppm clock crystals are presented. Fully-correlated equivalent channel taps offer a matrix $\mathbf{C}$ of ones, uncorrelated

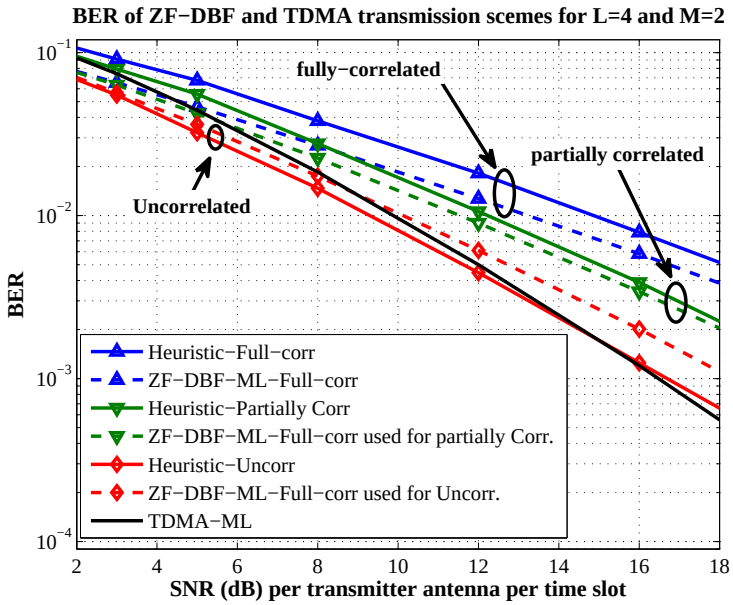

Figure 4.5: BER performance for ZF-DBF and TDMA transmission schemes including different cases of equivalent channel taps correlation.

equivalent channel taps create an identity covariance matrix $\mathbf{C}$ and partially correlated equivalent channel taps provide a matrix $\mathbf{C}$ with elements valued between 0 and 1.

For all the equivalent channel taps correlation types BER ZF-DBF detector (described in Eq. (3.3) and Eq. (2.20)) performance is provided. TDMA-based receiver is independent of any correlation, since coarse and fine correction of CFOs, $\{\Delta f_m\}_{m\in\mathcal{T}}$, is operated. For the partially correlated and uncorrelated equivalent channel taps case, the received samples are not totally affected by instantaneous deep fading or destructive addition of the transmitted signals compared to the fully-correlated case, since the correlation among the samples differs. In the case of ZF-DBF, ML detector is only provided for fully-correlated equivalent channel taps, thus heuristic receiver performs better for the uncorrelated case. On the other hand, ZF-DBF still remains better for the partially correlated equivalent channel taps. For low SNR regimes, heuristic receiver outperforms all the other schemes for the uncorrelated case, overcomes the reachback connectivity adversities.

Chapter 5

Conclusions and future work

5.1 Conclusions

This thesis focused on reachback connectivity problems, where one node cannot establish reliable communication towards the intended destination. Furthermore, no CSI acquisition exists, there is no available feedback from receiver and only low-cost off-the-self radio commodities are assumed.

Three concrete ZF-DBF non-coherent receivers were proposed: one heuristic receiver based on energy detection and two receivers (one maximum-likelihood and one heuristic) based on correlation of the equivalent channel taps. These proposed receivers exploit probabilistic alignment event in order to achieve constructive beamforming gain. Another receiver based on energy harvesting via a TDMA protocol among the receivers, collects energy in order to guarantee reliable connectivity at the destination. BER performance for the proposed receivers was computed via analytical and numerical methods.

It was shown that ZF-DBF scheme overcomes reachback connectivity adversities in low SNR regimes via signals' alignment of M distributed transmitters at the expense of power consumption; since only one node cannot reach the destination, because of power constraints. Nevertheless, at a high SNR regime, energy harvesting reception, using one node in a given time slot, performs better than the other schemes via multi-user diversity, where reachback connectivity adversities are not worth considering.

5.2 Future work

For the case of not fully-correlated (i.e., partially correlated and uncorrelated) equivalent channel taps, a maximum-likelihood non-coherent receiver needs

to be considered as future work. According to the analytical and numerical results of this thesis, easy-to-implement receivers were proposed. Implementation of this work using low-cost commodity radios can offer experimental validation of the theoretical results. A part of the implementation has been already initiated [33–37].

Appendix A

A.1 Circularly-symmetric complex Gaussian random vectors

A definition and a theorem for proper complex Gaussian random vectors are presented below:

Definition 1. *Complex jointly-Gaussian random vector* $\mathbf{v} = \mathbf{v}_R + \mathbf{v}_I$ *is circularly symmetric if* $e^{j\phi}\mathbf{v}$ *has the same probability distribution as* $\mathbf{v}$ *for all real* ϕ*.*

Corollary 1. *Since* $\mathbb{E}\left[e^{j\phi}\mathbf{v}\right] = e^{j\phi}\mathbb{E}\left[\mathbf{v}\right]$*, any circularly-symmetric complex random vector must have* $\mathbb{E}\left[\mathbf{v}\right] = \mathbf{0}$*, i.e., must have zero mean.*

Theorem 5. *Complex jointly-Gaussian random vector* $\mathbf{v}$ *is circularly symmetric if and only if* $\mathbf{M}_\mathbf{v} = \mathbb{E}\left[\left(\mathbf{v} - \mathbb{E}\left[\mathbf{v}\right]\right)\left(\mathbf{v} - \mathbb{E}\left[\mathbf{v}\right]\right)^T\right] = \mathbf{O}_n$*. In this case the p.d.f. of* $\mathbf{v}$ *is determined by its nonsingular covariance matrix* $\mathbf{\Sigma}_\mathbf{x}$ *and is given by [38, 39]:*

$$f_\mathbf{X}(\mathbf{x}) = \frac{1}{\pi^N \det\left(\mathbf{\Sigma}_\mathbf{x}\right)} \exp\left\{-\mathbf{x}^\dagger \mathbf{\Sigma}_\mathbf{x}^{-1}\mathbf{x}\right\}. \tag{A.1}$$

A.2 Gamma distribution

A random variable X is Gamma distributed, iff its pdf is given by:

$$f_X\left(x; k, \theta\right) = \frac{1}{\theta^k} \cdot \frac{1}{\Gamma(k)} \cdot x^{k-1} \cdot e^{-\frac{x}{\theta}} \cdot u(x), \tag{A.2}$$

where $u(\cdot)$ denotes the step function and $\Gamma(k) = (k-1)!$ for any positive integer.

A.3 Gaussian random vectors

The p.d.f. of a jointly-Gaussian random vector $\mathbf{x}$ with mean vector $\boldsymbol{\mu}$ and covariance matrix $\boldsymbol{\Sigma}$ is given by:

$$f_{\mathbf{X}}(\mathbf{x}) = \frac{1}{\sqrt{(2\pi)^N \det(\boldsymbol{\Sigma})}} \exp\left\{-\frac{1}{2}(\mathbf{x}-\boldsymbol{\mu})^T \boldsymbol{\Sigma}^{-1}(\mathbf{x}-\boldsymbol{\mu})\right\}. \tag{A.3}$$

Appendix B

B.1 PDF of the complex random variable g_l

Lemma 1. *The random variable* $g_l \triangleq \sum_{m=1}^{M} h_m e^{+j2\pi\Delta f_m l T_s}$, $\forall\, l \in \{1, 2, \ldots, L\}$, *is distributed according to* $\mathcal{CN}(0, M)$.

Proof. Given $\{\Delta f_m\}_{m\in\mathcal{T}}$, $g_l \sim \mathcal{CN}(0, M)$ as a linear combination of circularly-symmetric complex Gaussian random variables $\{h_m\}_{m\in\mathcal{T}} \sim \mathcal{CN}(0, 1)$. Thus, $f_{g_l|\{\Delta f_m\}_{m\in\mathcal{T}}}\left(g_l \mid \{\Delta f_m\}_{m\in\mathcal{T}}\right) \equiv \mathcal{CN}(0, M)$, which is independent of CFOs $\{\Delta f_m\}_{m\in\mathcal{T}}$. By taking the expectation over $\{\Delta f_m\}_{m\in\mathcal{T}}$, the p.d.f. of g_l is given by:

$$\begin{aligned} f_{g_l}(g_l) &= \mathbb{E}_{\mathbf{e}}\left[f_{g_l|\mathbf{e}}(g_l \mid \mathbf{e})\right] = f_{g_l|\mathbf{e}}(g_l \mid \mathbf{e}) \int_{-\infty}^{+\infty} f_{\mathbf{e}}(\mathbf{e})\, d\mathbf{e} \\ &= f_{g_l|\mathbf{e}}(g_l \mid \mathbf{e}), \end{aligned} \tag{B.1}$$

where $\mathbf{e} = \begin{bmatrix}\Delta f_1 & \ldots & \Delta f_M\end{bmatrix}^T$. □

B.2 CDF of a complex quadratic form $\mathbf{y}^\dagger \boldsymbol{\mathcal{A}} \mathbf{y}$

Lemma 2. *Let* $\mathbf{y}^\dagger \boldsymbol{\mathcal{A}} \mathbf{y}$ *the complex quadratic form of* $L \times 1$ $\mathbf{y}$, *where* $\mathbf{y} \sim \mathcal{CN}(\mathbf{0}, \boldsymbol{\mathcal{C}})$, $\boldsymbol{\mathcal{C}}$ *is real,* $\boldsymbol{\mathcal{A}}$ *is real and* $\boldsymbol{\mathcal{A}} = \boldsymbol{\mathcal{A}}^T$. *Then, the equivalent expression involving only real vectors is expressed as* $\widetilde{\mathbf{y}}^T \mathbf{E} \widetilde{\mathbf{y}}$, *where* $\widetilde{\mathbf{y}} \sim \mathcal{N}(\mathbf{0}, \boldsymbol{\Sigma})$, $\boldsymbol{\Sigma} = \begin{bmatrix} \frac{1}{2}\boldsymbol{\mathcal{C}} & 0_{L\times L} \\ 0_{L\times L} & \frac{1}{2}\boldsymbol{\mathcal{C}} \end{bmatrix}$ *and* $\mathbf{E} = \begin{bmatrix} \boldsymbol{\mathcal{A}} & 0_{L\times L} \\ 0_{L\times L} & \boldsymbol{\mathcal{A}} \end{bmatrix}$.

Proof. Let a complex random vector $\mathbf{y} \sim \mathcal{CN}(\mathbf{0}, \boldsymbol{\mathcal{C}})$, then the real-valued

equivalent random vector $\widetilde{\mathbf{y}}$ can be expressed as [39]:

$$\widetilde{\mathbf{y}} \triangleq \begin{bmatrix} \Re\{\mathbf{y}\}^T & \Im\{\mathbf{y}\}^T \end{bmatrix}^T \sim \mathcal{N}(\mathbf{0}, \boldsymbol{\Sigma}), \tag{B.2}$$

where the real covariance matrix $\boldsymbol{\Sigma} = \begin{bmatrix} \frac{1}{2}\Re(\boldsymbol{\mathcal{C}}) & -\frac{1}{2}\Im(\boldsymbol{\mathcal{C}}) \\ \frac{1}{2}\Im(\boldsymbol{\mathcal{C}}) & \frac{1}{2}\Re(\boldsymbol{\mathcal{C}}) \end{bmatrix}$.

Since matrix $\boldsymbol{\mathcal{C}}$ is real, the covariance matrix of $\widetilde{\mathbf{y}}$ is given by $\boldsymbol{\Sigma} = \begin{bmatrix} \frac{1}{2}\boldsymbol{\mathcal{C}} & 0_{L\times L} \\ 0_{L\times L} & \frac{1}{2}\boldsymbol{\mathcal{C}} \end{bmatrix}$.

Using Eq. (B.2) the real-equivalent of complex vector $\mathbf{y} \sim \mathcal{CN}(\mathbf{0}, \boldsymbol{\Sigma})$ can be written as $\widetilde{\mathbf{y}} = \begin{bmatrix} \Re\{\mathbf{y}\}^T & \Im\{\mathbf{y}\}^T \end{bmatrix}^T \sim \mathcal{N}(\mathbf{0}, \boldsymbol{\Sigma})$.

Define $\mathbf{y}_R \triangleq \Re\{\mathbf{y}\}$ and $\mathbf{y}_I \triangleq \Im\{\mathbf{y}\}$, then:

$$\begin{aligned} \mathbf{y}^\dagger \boldsymbol{\mathcal{A}} \mathbf{y} &= \left(\mathbf{y}_R^T - j\mathbf{y}_I^T\right) \boldsymbol{\mathcal{A}} \left(\mathbf{y}_R + j\mathbf{y}_I\right) \\ &= \mathbf{y}_R^T \boldsymbol{\mathcal{A}} \mathbf{y}_R + j\mathbf{y}_R^T \boldsymbol{\mathcal{A}} \mathbf{y}_I - j\mathbf{y}_I^T \mathbf{A} \mathbf{y}_R + \mathbf{y}_I^T \boldsymbol{\mathcal{A}} \mathbf{y}_I, \\ \widetilde{\mathbf{y}}^T \mathbf{E} \widetilde{\mathbf{y}} &= \mathbf{y}_R^T \boldsymbol{\mathcal{A}} \mathbf{y}_R + \mathbf{y}_I^T \boldsymbol{\mathcal{A}} \mathbf{y}_I. \end{aligned}$$

Thus, iff $\boldsymbol{\mathcal{A}} = \boldsymbol{\mathcal{A}}^T$, then $\mathbf{y}^\dagger \boldsymbol{\mathcal{A}} \mathbf{y} = \widetilde{\mathbf{y}}^T \mathbf{E} \widetilde{\mathbf{y}}$. □

Using Lemma 2, $\mathbf{y}^\dagger \boldsymbol{\mathcal{A}} \mathbf{y} \equiv \widetilde{\mathbf{y}}^T \mathbf{E} \widetilde{\mathbf{y}}$, and thus, using [40, Theorem 4.2b.1], the c.d.f. is given by:

$$F_r(\boldsymbol{\lambda}, z) = \sum_{i=0}^{+\infty} (-1)^i c_i \frac{z^{\frac{r}{2}+i}}{\Gamma\left(\frac{r}{2}+i+1\right)} \tag{B.3}$$

where $\Gamma(z) = \int_0^{+\infty} t^{z-1} e^{-t} dt$ denotes the Gamma function, $r = \operatorname{rank}(\mathbf{E})$ and vector $\boldsymbol{\lambda} = \begin{bmatrix} \lambda_1 & \cdots & \lambda_r \end{bmatrix}^T$ contains the eigenvalues of $2L \times 2L$ matrix $\boldsymbol{\Sigma}^{\frac{1}{2}} \mathbf{E} \boldsymbol{\Sigma}^{\frac{1}{2}}$.

The coefficients c_i $(i \geq 0)$ can be calculated recursively through the relation:

$$c_i \triangleq \begin{cases} \prod_{j=1}^{r} (2\lambda_j)^{-\frac{1}{2}}, & i = 0, \\ \frac{1}{i} \sum_{j=0}^{i-1} d_{i-j} c_j, & i > 0, \end{cases} \tag{B.4}$$

where d_i $(i \geq 1)$ is expressed as follows:

$$d_i \triangleq \frac{1}{2} \sum_{j=1}^{r} (2\lambda_j)^{-i}, \qquad i \geq 1. \tag{B.5}$$

Bibliography

[1] N. D. Sidiropoulos, T. N. Davidson, and Z. Q. Luo, "Transmit beamforming for physical layer multicasting," *IEEE Trans. Signal Processing*, vol. 54, no. 6, pp. 2239–2251, Jun. 2006.

[2] V. H. Nassab, S. Shahbazpanahi, A. Grami, and Z. Q. Luo, "Distributed beamforming for relay networks based on second-order statistics of the channel state information," *IEEE Trans. Signal Processing*, vol. 56, no. 9, pp. 4306–4316, Sep. 2008.

[3] Y.-S. Tu and G. Pottie, "Coherent cooperative transmission from multiple adjacent antennas to a distant stationary antenna through awgn channels," in *IEEE 55th Vehicular Technology Conf. (VTC)*, vol. 1, 2002, pp. 130–134.

[4] R. Mudumbai, J. Hespanha, U. Madhow, and G. Barriac, "Scalable feedback control for distributed beamforming in sensor networks," in *IEEE International Symp. on Information Theory (ISIT)*, 2005, pp. 137–141.

[5] R. Mudumbai, G. Barriac, and U. Madhow, "On the feasibility of distributed beamforming in wireless networks," *IEEE Trans. Wireless Commun.*, vol. 6, no. 5, pp. 1754–1763, May 2007.

[6] D. Brown and H. Poor, "Time-slotted round-trip carrier synchronization for distributed beamforming," *IEEE Trans. Signal Processing*, vol. 56, no. 11, pp. 5630–5643, 2008.

[7] D. Brown and R. Preuss, "Retrodirective distributed transmit beamforming with two-way source synchronization," in *44th Annual Conference on Information Sciences and Systems (CISS)*, 2010, pp. 1–6.

[8] R. Mudumbai, B. Wild, U. Madhow, and K. Ramchandran, "Distributed beamforming using 1 bit feedback: From concept to realization," in *Proc. Allerton Conf. on Communication, Control and Computing*, Sep. 2006, pp. 1020–1027.

[9] R. Mudumbai, J. Hespanha, U. Madhow, and G. Barriac, "Distributed transmit beamforming using feedback control," *IEEE Trans. Inform. Theory*, vol. 56, no. 1, pp. 411–426, Jan. 2010.

[10] S. Sigg and M. Beigl, "Algorithms for closed-loop feedback based distributed adaptive beamforming in wireless sensor networks," in *IEEE 5th International Conference on Intelligent Sensors, Sensor Networks and Information Processing (ISSNIP)*, 2009, pp. 25–30.

[11] M. Seo, M. Rodwell, and U. Madhow, "A feedback-based distributed phased array technique and its application to 60-ghz wireless sensor network," in *IEEE MTT-S International Microwave Symposium Digest*, 2008, pp. 683–686.

[12] Y. Zhang, X. Li, and M. Amin, "Distributed beamforming in multi-user cooperative wireless networks," in *Proc. 4th Int. Conf. Commun. Network. China (ChinaCOM)*, Aug. 2009, pp. 1–5.

[13] Y. Jing and H. Jafarkhani, "Beamforming in wireless relay networks," in *Proc. Inf. Theory Appl. Worksh.*, 2008, pp. 142–150.

[14] A. Kalis and A. Kanatas, "Cooperative beamforming in smart dust: Getting rid of multihop communications," *IEEE Pervasive Computing*, vol. 9, no. 3, pp. 47–53, 2010.

[15] H. Balan, R. Rogalin, A. Michaloliakos, K. Psounis, and G. Caire, "Airsync: Enabling distributed multiuser mimo with full spatial multiplexing," vol. 21, no. 6, pp. 1681–1695, Dec. 2013.

[16] F. Quitin, M. Rahman, R. Mudumbai, and U. Madhow, "A scalable architecture for distributed transmit beamforming with commodity ra-

dios: design and proof of concept," vol. 12, no. 3, pp. 1418–1428, Mar. 2013.

[17] J. Uher, T. Wysocki, and B. Wysocki, "Review of distributed beamforming," *Journal of Telecommunications and Information Technology*, 2011.

[18] Y. Lebrun, K. Zhao, S. Pollin, A. Bourdoux, F. Horlin, and R. Lauwereins, "Performance analysis of distributed ZF beamforming in the presence of CFO," *EURASIP Journal on Wireless Communications and Networking*, Nov 2011.

[19] S. Chatzinotas, S. K. Sharma, and B. Ottersten, "Asymptotic analysis of eigenvalue-based blind spectrum sensing techniques," in *Proc. of the 2013 IEEE Int. Conference on Acoustics, Speech and Signal Processing, ICASSP 2013*, May 2013, pp. 4464–4468.

[20] Y. Zeng and Y.-C. Liang, "Maximum-minimum eigenvalue detection for cognitive radio," in *IEEE 18th International Symposium on Personal, Indoor and Mobile Radio Communications, PIMRC 2007*, 2007, pp. 1–5.

[21] ——, "Eigenvalue-based spectrum sensing algorithms for cognitive radio," *IEEE Trans. Commun.*, vol. 57, no. 6, pp. 1784–1793, 2009.

[22] C. G. Tsinos and K. Berberidis, "Adaptive eigenvalue-based spectrum sensing for multi-antenna cognitive radio systems," in *Proc. of the 2013 IEEE Int. Conference on Acoustics, Speech and Signal Processing, ICASSP 2013*, May 2013, pp. 4454–4458.

[23] T. L. Marzetta and B. M. Hochwald, "Capacity of a mobile multiple-antenna communication link in rayleigh flat fading," *IEEE Trans. Inform. Theory*, vol. 45, pp. 139–157, Jan. 1993.

[24] B. M. Hochwald and T. L. Marzetta, "Unitary space-time modulation for multiple-antenna communication in rayleigh flat-fading," *IEEE Trans. Inform. Theory*, vol. 46, pp. 543–564, Mar. 2000.

[25] B. Hochwald, T. Marzetta, T. Richardson, W. Sweldens, and R. Urbanke, "Systematic design of unitary space-time constellations," *IEEE Trans. Inform. Theory*, vol. 46, no. 6, pp. 1962–1973, Sep. 2000.

[26] K. Alexandris, "Distributed zero-feedback beamforming for emergency radio," Diploma Thesis, Technical University of Crete, Chania, Greece, Sep. 2012, http://users.isc.tuc.gr/~kalexandris/theses.html.

[27] A. Bletsas, A. Lippman, and J. Sahalos, "Simple, zero-feedback, distributed beamforming with unsynchronized carriers," *IEEE J. Select. Areas Commun.*, vol. 28, no. 7, pp. 1046–1054, Sep. 2010.

[28] ——, "Zero-feedback, collaborative beamforming for emergency radio: Asymptotic analysis," *Mobile Networks and Applications (MONET)*, vol. 16, no. 5, pp. 589–599, Oct. 2011.

[29] M. S. Alouini, A. Abdi, and M. Kaveh, "Sum of gamma variates and performance of wireless communication systems over nakagami-fading channels," *IEEE Trans. Veh. Technol.*, vol. 50, no. 6, pp. 1471–1480, Nov. 2001.

[30] J. F. Paris, "A note on the sum of correlated gamma random variables," Mar. 2011, arXiv:1103.0505.

[31] M. Abramowitz and I. A. Stegun, *Handbook of Mathematical Functions with Formulas, Graphs, and Mathematical Tables*. New York: Dover, 1964.

[32] F. W. Olver, D. W. Lozier, R. F. Boisvert, and C. W. Clark, *NIST Handbook of Mathematical Functions*, 1st ed. New York, NY, USA: Cambridge University Press, 2010.

[33] K. Alexandris, G. Sklivanitis, and A. Bletsas, "Reachback wsn connectivity: Non-coherent zero-feedback distributed beamforming or tdma energy harvesting?" under submission.

[34] G. Sklivanitis and A. Bletsas, "Testing zero-feedback distributed beamforming with a low-cost SDR testbed," in *2011 Conference Record of the Forty Fifth Asilomar Conference on Signals, Systems and Computers (ASILOMAR)*, Nov. 2011, pp. 104–108.

[35] G. Sklivanitis, "Disruptive communications," Master's thesis, ECE Department, Technical University of Crete, Chania, Greece, under preparation.

[36] G. Sklivanitis, K. Alexandris, and A. Bletsas, "Testbed for non-coherent zero-feedback distributed beamforming," in *Proc. of the 2013 IEEE Int. Conference on Acoustics, Speech and Signal Processing, ICASSP 2013*, May 2013, pp. 2563–2567.

[37] K. Alexandris, G. Sklivanitis, and A. Bletsas, "Non-coherent receivers for zero-feedback distributed beamforming with commodity radio," in *IEEE Global Telecommunications Conference (GLOBECOM 2014)*, under submission.

[38] F. Nesser and J. Massey, "Proper complex random processes with applications to information theory," *IEEE Trans. Inform. Theory*, vol. 39, no. 7, pp. 1293–1302, Jul. 1993.

[39] R. Gallager, "Circularly-symmetric gaussian random vectors," Jan. 2008, http://www.rle.mit.edu/rgallager/documents/CircSymGauss.pdf.

[40] A. Mathai and S. Provost, *Quadratic Forms in Random Variables: Theory and Applications*, ser. Statistics: A Series of Textbooks and Monographs. Marcel Dekker Incorporated, 1992.